Journal of Materials Chemistry C

PAPER

View Article Online
View Journal | View Issue

Cite this: J. Mater. Chem. C, 2014, 2, 8880

Plasmonic enhancement of dual mode fluorescence in a silver nano-antenna–ZnO:Er^{3+} hybrid nanostructure†

Rupali Das, Parikshit Phadke, Naveen Khichar and Santa Chawla*

Received 8th July 2014
Accepted 30th August 2014

DOI: 10.1039/c4tc01479k

www.rsc.org/MaterialsC

Tuning of surface plasmon resonance (SPR) of silver nanoparticles (Ag NPs) through shape tailoring make them frequency tunable multipolar optical nano antennas that can be harnessed for optical enhancements in a fluorophore placed in optimal proximity. Such SPR tuning has been achieved with Ag nano-hexagons in which enhancements in both down (under UV excitation) and up (under IR excitation) conversion fluorescence from rare earth Er^{3+}–doped ZnO nanoparticles are realised. The near field generated by the pure Ag NPs and their hybrids under UV and IR incident light is simulated using a finite difference time domain method, and a direct correlation with the observed fluorescence enhancement is established.

Introduction

Shape-tailored noble metal nanoparticles (MNPs) have the distinctive ability to confine and enhance the incident electromagnetic (EM) field around them through the coherent collective oscillation of surface electrons (termed surface plasmon resonance (SPR)) in distinct dipolar and multipolar modes[1] as well as the lightening rod effect. MNPs such as silver nanoparticles (Ag NPs) can thus behave like multipolar optical nanoantennas, and their SPR modes can be tuned through the tailoring of shape, size and dielectric environment. The near field of Ag NPs can couple to either the excitation or emission frequencies of a fluorophore placed at a proximal distance, leading to fluorescence enhancement[2] where the SPR of Ag NPs must overlap with either the absorption or emission band of the fluorophore. The coupling of metal semiconductor hybrid nanostructures at optical frequencies for enhanced performance is of particular interest for applications such as solar cells, solid state lighting, biological imaging, *etc.* For these coupled hybrid systems to be effective, the tailoring and matching properties of both constituent components is extremely important. Direct band gap semiconductors like ZnO have a great advantage in this regard as they are excellent emitters in the UV-visible region and can also accommodate discrete 4f levels of light emitting trivalent rare earth (RE) ions in their wide forbidden gap to tune the excitation and emission ranges. Despite the importance of ZnO as tunable light emitter, reports on ZnO–MNP hybrids for fluorescence enhancement are rare.[3–9] The designed EM field of shape- and size-tailored Ag NPs has been shown to have a significant role in the fluorescence enhancement of RE ions.[10–12] In metal semiconductor hybrid nanostructures, surface plasmon modes and wave functions of bound excitons can remain unperturbed in the weak coupling region, and the interaction of the plasmon EM field with the

Luminescent Materials Group, CSIR-National Physical Laboratory, Dr. K. S. Krishnan Road, New Delhi-110012, India. E-mail: santa@nplindia.org

† Electronic supplementary information (ESI) available: *Sample synthesis*: trivalent rare earth Er^{3+} (2 atomic%)–doped ZnO nanoparticles were synthesised by co-precipitation (CPP) at room temperature using sub-molar precursor solutions of zinc acetate and erbium nitrate in an alkaline environment (pH 10). The silver nanoparticles were synthesized using optimal concentrated solutions of $AgNO_3$, PVP and tri-sodium citrate. The desired shapes and sizes of the nanoparticles were tailored using optimised concentrations of $NaBH_4$ as well as H_2O_2 (30% w/v). *UV-visible absorption measurements*: the absorption spectra of the Ag NP solutions were measured by an Avantes UV-visible spectrometer. *Thickness measurement*: the thickness of the PVA film was measured with a Stylus Profilometer (Ambios XP200). *Fluorescence measurements*: confocal fluorescence microscopy (WITec alpha 300M+) was employed to study the hybrid thin film material system with an 100× microscope objective (N.A 0.9) and UV diode laser (output $\lambda \sim 375$ nm, power 10 mW, Toptica) excitation source. The upconversion photo luminescence measurements in the ZnO:Er^{3+} and Ag NP conjugated samples were performed using a power tunable 980 nm diode laser (MDL-N-980-6W) coupled with an optical fibre as an excitation source and an Edinburgh Instruments fluorescence spectrometer (FLSP920). Time-resolved photoluminescence (PL) decay was measured using an Edinburgh Instruments time resolved spectrometer (FLSP920) with a pulsed Xe lamp as an excitation source and a time-correlated single photon counting (TCSPC) technique. *FDTD simulation*: the calculation of near field and extinction properties of a silver nano-hexagon was done using an FDTD method (Lumerical FDTD solutions 8.7.1). The refractive index of the surrounding medium was kept at 1.33. We used the Conformal Variant 1 mesh refinement option and standard PML boundaries to prevent reflections from absorbing boundaries. We used a broadband total field scattering field (TFSF) source and implemented suitable monitors to calculate the near field and extinction properties of silver nano-hexagons. A plane wave source as the incident optical field was injected from the *Z*-axis, which falls perpendicular to the silver nano-hexagons resting on a plane; this configuration exactly conforms to the experimental setup used for confocal fluorescence measurements. Fig. S1 XRD pattern of ZnO:Er^{3+}. Fig. S2 SEM and TEM images of ZnO:Er^{3+} and TEM image of Ag NPs. Fig. S3 PL excitation spectrum of ZnO:Er^{3+}. Fig. S4 FDTD simulated absorption and scattering spectra of Ag NPs by injecting incident light from the *X*, *Y* direction and the real and imaginary part of the dielectric function of Ag NP (from Palik's model) and the corresponding FDTD model fit. See DOI: 10.1039/c4tc01479k

emitting dipole can lead to enhanced absorption when the SPR matches with the absorption band of the semiconductor NP. Undoped ZnO has excitation in the UV region (band edge excitation ~370 nm) and emission in the visible region due to the recombination of electron–hole pairs in intrinsic defects. ZnO NPs can be made into upconversion (UC) luminescence emitters by doping with the appropriate lanthanide ion such as erbium (Er^{3+}), which can absorb infrared (IR) light due to the transition between its discrete 4f levels ($^4I_{15/2}$–$^4I_{11/2}$). Hence, Er^{3+} doping in ZnO NPs could make them dual absorbers of both UV and IR EM radiation, with visible, intrinsic emission under UV and characteristic green/red Er^{3+} UC luminescence under IR excitation. In order to achieve enhanced dual mode luminescence from such ZnO:Er^{3+} NPs in a metal semiconductor hybrid nanostructure, the SPR of a metal (Ag NPs) has to be tuned to match both the excitation range in UV and IR. Photoluminescence (PL), however, is often quenched due to non-radiative charge transfer processes between semiconductor and metal particles in direct contact. To enhance plasmon-bound exciton interactions, a dielectric spacer layer in the form of linker molecules must be introduced for effective separation and to avoid luminescence quenching. To achieve this, we have used colloid chemistry to fabricate shape- and size-tailored Ag NPs for tuning the SPR as well as to attach specific linker molecules to the Ag NPs.

In the present work, we explore the multipolar character of silver nano-hexagons and employ quadrupolar and dipolar SPR modes in the UV and IR regions to couple with the specific excitation energy of RE ion (Er^{3+})–doped ZnO nanoparticles to achieve dual mode luminescence enhancement. The novelty of this work lies in the tuning of the surface plasmon modes by shape-tailoring silver nanoparticles and coupling such modes with fluorescent nanoparticles in both the UV and IR spectral regions to harness optical enhancement in the visible region; this enhancement has immense importance from the point of view of developing optical devices. Plasmon enhanced fluorescence from Er^{3+} has been reported for gold nanowire-$NaYF_4$:Yb, Er,[13] Ag–SiO_2–Y_2O_3:Er nanostructure,[14] gold nanosphere–$NaYF_4$:Yb, Er nanocrystals,[15] and Ag NP–bismuth germanate glasses.[16] To the best of our knowledge, no work has been reported on dual mode luminescence enhancement in doped ZnO–Ag NP hybrid structures or any other fluorophore. We report the luminescence enhancement in both down- and up-conversion emissions from Er^{3+}–doped ZnO nanoparticles in the proximity of SPR-tuned Ag NPs. In order to comprehend the correlation of fluorescence enhancement with the multipolar near field generated around Ag NPs, FDTD simulation was carried out for representative Ag nano-hexagons and their hybrids under UV and IR incident radiation, and a cause–effect relationship was established.

Experimental

Trivalent rare earth Er^{3+} (2 atomic%)–doped ZnO nanoparticles were synthesised by co-precipitation (CPP) at room temperature using sub-molar precursor solutions of zinc acetate and erbium nitrate. The CPP technique ensured the effective incorporation of dopant in nano-sized ZnO. XRD confirmed the monophasic wurtzite hexagonal ZnO structure [see ESI Fig. S1†]. The morphological analysis revealed hierarchical flower-like formations (Fig. 1a). The inset in Fig. 1b shows the magnified TEM image of a single flower comprising individual nanoparticles (~5 nm), as revealed in the HRTEM image showing well-formed lattice fringes (Fig. 1b) [see ESI Fig. S2†]. Ag NPs were synthesised by optimising the method developed by Meutrax and Mirkin[17] to yield an Ag NP solution with blue colour, which is a consequence of its SPR band. The solution is composed mostly of polygonal (hexagonal-like) Ag NPs with edge lengths of ~50 nm, as evident from the collage of TEM images (Fig. 1c). The typical thickness of the nano-hexagons is about 25 nm, as measured from TEM micrographs. The ZnO:Er^{3+} and Ag NPs integrated hybrid nanostructure in a thin film configuration was prepared by controlled drop casting on a microscope cover slip. The material system was conjugated by first drop casting a thin layer of ZnO:Er^{3+} nanoparticles dispersed in PVA (3% PVA in water) on the substrate followed by a thin layer of Ag NPs. The PVA spacer layer prevents the formation of any silver oxide at the AgNP–ZnO:Er^{3+} interface due to oxidation as well as the quenching of fluorescence due to

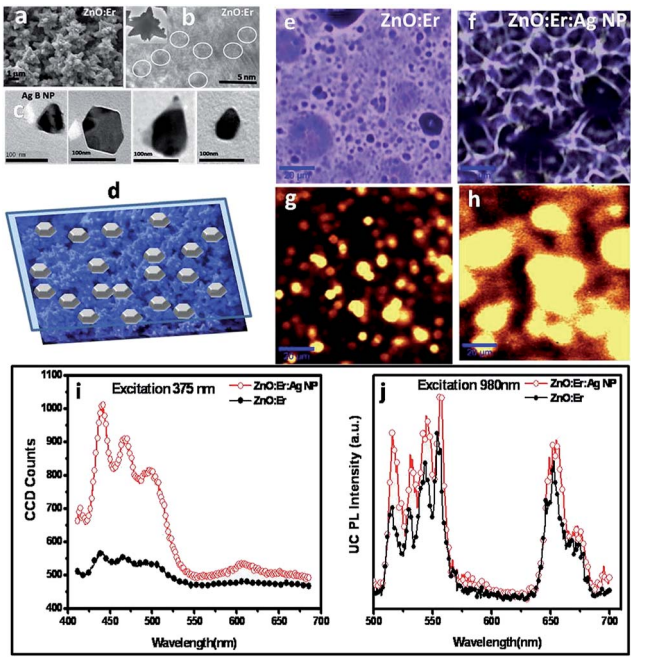

Fig. 1 SEM image of flower-like ZnO:Er^{3+} (a); HRTEM image showing the lattice fringes of individual ZnO:Er^{3+} nanoparticles (b), inset shows the TEM image of single nano-flower; collage of TEM images of Ag NPs (c); graphical representation (not to scale) of the integrated ZnO:Er^{3+} (blue flowers, SEM image), PVA layer (blue transparent layer) and Ag NPs (metallic silver hexagons) hybrid structure used for the confocal fluorescence study (d). Optical image and corresponding confocal fluorescence image of ZnO:Er^{3+} (e) & (g) and the ZnO:Er^{3+}–Ag NP hybrid (f) & (h) under 375 nm UV excitation; the corresponding confocal fluorescence (integrated) spectra under 375 nm laser excitation (i) and the UC PL spectra of the ZnO:Er^{3+} (black curve) and ZnO:Er^{3+}–Ag NP hybrid structures (red curve) under 980 nm laser excitation (j).

intervening non-radiative transitions when Ag NPs are placed in the proximity of the fluorescent NPs.[18] The deposition and conjugation parameters for the dielectric spacer layer were optimized to realise metal-enhanced fluorescence. The thickness of the PVA spacer layer as measured by optical profilometry is about 100 nm. Systematic studies of PVA concentration and layer deposition parameters for metal-enhanced fluorescence have been reported,[11,12] and in most inorganic nanoparticles and Ag NP combinations, the spacer layer thickness employed in the present study produces good results. The graphical representation of the ZnO:Er^{3+} nano-flower–PVA layer–Ag NPs integrated thin film system used for confocal fluorescence microscopy is shown in Fig. 1d to clearly show the different components in the integrated material system. The light is incident perpendicularly in the experimental arrangement.

Results and discussion

The optical (Fig. 1e and f) and corresponding confocal fluorescence images (Fig. 1g and h) of ZnO:Er^{3+} and ZnO:Er^{3+}–Ag NPs integrated system under UV (375 nm) excitation clearly show regions of bright fluorescence as well as greater emission intensity from ZnO:Er^{3+} in proximity to Ag NPs (Fig. 1h). The corresponding integrated emission spectra (Fig. 1i) of ZnO:Er^{3+} in propinquity to Ag NPs (predominantly hexagonal Ag NPs with sizes of ~50 nm) clearly show enhancements in fluorescence of up to 546% (at 442 nm) compared to ZnO:Er^{3+} under UV excitation. This significant fluorescence enhancement can be attributed to the plasmonic coupling of the EM field of the Ag NPs[19] with the bound excitons of the ZnO nanoparticles.[20]

The measured upconversion photoluminescence (PL) emission spectra of the hybrid nanostructure of ZnO:Er^{3+} with Ag NPs under 980 nm laser excitation is shown in Fig. 1j, displaying both green and red UC emission. The spectrum reveals enhancement in the emission intensity when ZnO:Er^{3+} nanoparticles are conjugated with Ag NPs in the hybrid system. The UC fluorescence enhancement due to the plasmonic effect is 174.5% for the 516 nm peak, 152.8% for the 531 nm peak, 132.6% for the 545 nm peak and 115.7% for the 655 nm red peak compared to ZnO:Er^{3+} under IR excitation. As the emission wavelength increases, partial absorption of the emitted fluorescence by Ag NPs can occur, as their absorption becomes strong in that spectral region (Fig. 2c). Hence, the enhancement is lower at the 655 nm emission wavelength.

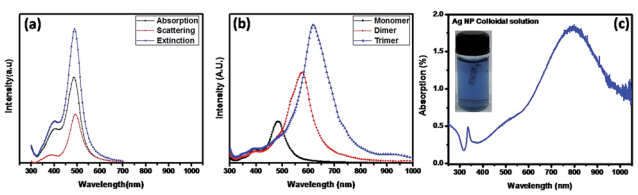

Fig. 2 FDTD simulated absorption, scattering and extinction spectra of Ag nano-hexagons (a), the shift in extinction spectra from monomer to dimer to trimer (b), and the experimental UV-visible absorption spectrum of the Ag NP colloidal solution (c), the inset shows an actual photograph of the colloidal solution.

Ag nanowire-enhanced upconversion emission has been reported for the $NaYF_4$:Yb^{3+}, Er^{3+} system[21] and $NaYF_4$:Yb^{3+}/Tm^{3+} coated with Au nanoparticles,[22] but no such report is available for UC enhancement in RE-doped ZnO. This study clearly indicates that the upconversion emission in ZnO can be enhanced by SPR-tuned Ag NPs. The Ag NPs localize the incident EM field in different plasmonic modes and the near field around them contributes to the fluorescent enhancements. The measured UV-visible absorption spectrum of the Ag NP colloidal solution (Fig. 2c) exhibits a quadrupolar resonance peak at 335 nm, which covers the excitation range of ZnO:Er^{3+} (ESI Fig. S3†). The broad dipolar peak centred at 795 nm extends up to 1000 nm in the absorption spectrum. The well-matched spectral overlap of the excitation range of upconversion nanoparticles, as revealed in the measured absorption spectrum of the Ag NPs in the near-IR region (Fig. 2c), clearly suggests the excitation enhancement leading to UC fluorescence enhancement.

To elucidate the influence of the near field generated around the differently-shaped Ag NPs used in the experiments on fluorescence enhancement, three-dimensional finite difference time domain (FDTD) simulations of the pure Ag NPs and their hybrids were carried out. One Ag NP from the solution was considered for the simulation on the basis of the average geometrical distribution. A representative Ag nano-hexagon was chosen, and its image was imported from the transmission electron micrograph for FDTD simulation. The FDTD technique has been proven to solve Maxwell's electromagnetic equation for plasmonic structures with complex geometries; it considers both the $E(t)$ and $H(t)$ components discretely over time.[23] The steady-state continuous wave field $E(\omega)$ is then calculated by Fourier transformation of $E(t)$ during the simulations. All simulations were performed with light injected along the Z-axis, which is perpendicular to the thin film, thus conforming to the experimental setup. FDTD solutions (version 8.7.1)[24] was employed to perform the simulations with a mesh size of 0.8 nm to obtain results with a high degree of accuracy. The material response was taken from Palik[25] (0–2 μm), and the field was allowed to evolve for 200 fs. The FDTD method was employed to calculate the absorption, scattering and extinction spectra for the Ag nano-hexagon (Fig. 2a). In the experimental setup, a number of Ag NPs and their aggregates are deposited on the ZnO:Er^{3+} NPs. To estimate such effects of plasmonic coupling between closely-spaced Ag NPs, particle hybrids such as dimers and trimers were simulated in a linear arrangement with an inter-particle separation of 5 nm. The extinction spectra for the nano-hexagon dimer and trimer (~50 nm, separated by 5 nm) were also calculated to elucidate the effect of particle hybrids (Fig. 2b). As the particle size of the hexagonal Ag NP is about 50 nm, non-radiative damping due to electron–phonon interaction resulting in absorption as well as radiative resonant scattering of plasmon modes are operative.[26] For a single nano-hexagon, the extinction peak is at 488 nm; this peak red shifts to 576 nm for the dimer and 616 nm for the trimer. It is also known from FDTD simulation that as the number of particles in a particle hybrid system increases, the extinction spectrum broadens and red shifts[26,27] due to interaction of plasmonic modes of neighbouring Ag NPs.[12] Moreover, the formation of clusters or closely

spaced nanoparticle hybrids in the film leads to the coupling of plasmon modes and the enhancement of the local EM field.[11,12] In near field coupling between Ag NPs, the restoring force operative upon the oscillating electron cloud of individual NPs could increase or decrease based on the charge distribution of the proximate particles. In a longitudinal array of Ag NPs, red shifts of the SPR of longitudinal modes can occur.[28] The absorption spectrum of the Ag NP colloidal solution, as measured by UV-visible spectroscopy (Fig. 2c), represents the absorption profile of a random distribution of Ag NPs in a homogenized medium. The observed broad absorption peak can be attributed to the inhomogeneous damping caused by different spatial positions and random orientations of Ag NPs in colloidal solution, which gives rise to different peak positions; the broad curve can be understood as a convolution of all the resulting peaks (see ESI S4†).[11]

For a quantitative comparison of the effect of Ag NPs on the rare earth-doped ZnO particles, the FDTD method was employed to calculate the generated EM field of the hexagonal Ag NP at excitation wavelengths of 375 nm, 980 nm and at the localized surface plasmon resonance (LSPR) frequency. Near field images of the simulated EM field ($|E|$) of the Ag nano-hexagon (Fig. 3a–c) and dimers (Fig. 3d–f) at 375 nm, 795 nm (LSPR) and 980 nm undoubtedly show hotspots due to diploar and quadrupolar modes and the lightening rod effect.

The local electric field values $|E|^2$ listed in Table 1 show that the largest $|E|^2$ values obviously occur at the dipolar LSPR frequency. At an excitation wavelength of 375 nm, the calculated $|E|^2$ value for the Ag nano-hexagon is 19 times that of the incident field. However, when the wavelength of incident light is 980 nm, the $|E|^2$ value is calculated to be 11 times that of the Ag NP.[12] Thus, the simulated near field images of the pure Ag NP clearly elucidate the confined near field under different excitation wavelengths. The field enhancement for the dimer increases 295 times, 63 times and 22 times that of the incident EM field at SPR, 375 nm and 980 nm, respectively. The field enhancement for the dimer is 2–3 times that of monomer at incident optical fields of different frequencies (Table 1). Such *E*-field enhancements occur due to the confinement of the field in the intergap region of Ag NPs as well as around them, as is clearly elucidated in Fig. 3d–f.[29] Larger enhancements are expected for larger ensembles of particles. Such a collection of Ag NP has also been used to explain metal-enhanced fluorescence in ZnMgO.[30]

Table 1 Near field enhancement of Ag nano-hexagon

E-field enhancement $\|E\|^2$ (*Z*-direction)			
Ag NP	SPR	375 nm	980 nm
Monomer	112	19	11
Dimer	295	63	22

The near field enhancements of Ag NPs and their hybrids at UV and IR excitation wavelengths are thus commensurate with the observed fluorescence enhancement at these respective excitation wavelengths corresponding to down and upconversion emission from ZnO:Er^{3+} (Fig. 1i and j). The strong near field generated by Ag NPs enhances the total electric field experienced by Er^{3+} ions, and the non-linear optical process leading to upconversion emission is enhanced as the radiative transitions of Er^{3+} ions originate from electric dipoles. The coupling of the excited state of Er^{3+} and the Ag NP dipolar LSPR modifies the Stark shift.[29] As a result of change in local electric field adjacent to RE ions due to coupling with Ag NPs, the emission peaks are red shifted (Fig. 1j) by a few nm with an appreciable increase in luminescence. The $|E|^2$ values obtained from FDTD solutions of Ag NP monomer and dimer under a 980 nm incident field clearly reveal a correlation between the generated near field and the enhancement in UC luminescence.

It is well known that metal-enhanced fluorescence can occur through excitation enhancement (enhancement of local EM field) and/or through emission enhancement (enhancement of radiative decay rate). However, it is difficult to distinguish between the contributions of these two components, particularly when the broad SPR band of Ag NPs (Fig. 2c) overlap with both the excitation and emission spectra of ZnO:Er^{3+} nanoparticles. Excitation enhancement produces a higher excitation rate, but does not change the lifetime of the fluorophore. On the other hand, emission enhancement increases the radiative decay rate, reducing the luminescence decay time.[31] We have measured the luminescence decay under 375 nm excitation (Fig. 4) for Ag NPs conjugated with ZnO:Er^{3+} nanoparticles; the decay characteristics remain similar with and without Ag NPs. This suggests that the prominent mechanism for visible fluorescence enhancement in ZnO:Er^{3+} is the enhancement of near field due to presence of Ag NPs in proximity through excitation enhancement. If the scattering of metal nanoparticles is responsible for such fluorescence enhancement, then scattering spectra must reflect this spectral dependence. The FDTD-calculated scattering spectra (Fig. 2a) show maxima around 500 nm and negligible scattering at 442 nm, where we observed 546% enhancement. Moreover, it is well known that scattering contributes to emission enhancement when the LSPR band overlaps with the emission spectra of the fluorophore;

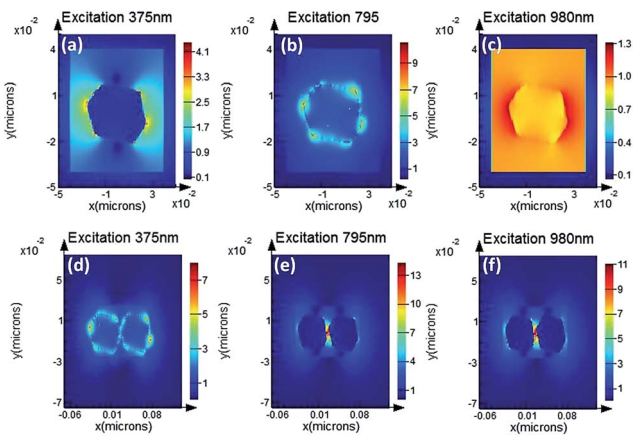

Fig. 3 Near field ($|E|$) images at different incident wavelengths by FDTD simulation of an exact Ag nano-hexagon and dimers.

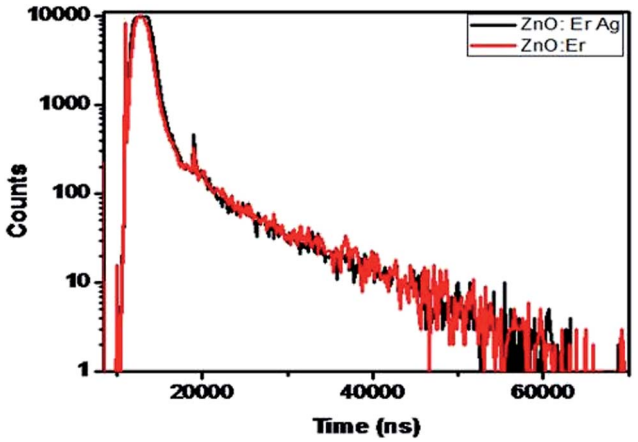

Fig. 4 Luminescence decay curve of blue emission under 375 nm excitation.

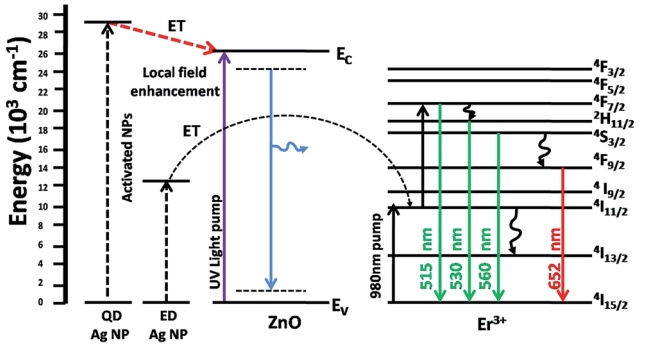

Fig. 5 Energy level diagram showing Ag NP excitation and energy transfer (ET) corresponding to quadrupolar resonance (QD) to ZnO under UV pump and also the ET corresponding to dipolar resonance (ED) from Ag NP to Er^{3+} levels under 980 nm pump laser. The emission transitions are indicated by downward arrows.

confirmation of this effect comes from the measurement of luminescence decay, where emission enhancement increases the radiative decay rate, thus reducing the luminescence decay time. Our experimental decay measurements (Fig. 4), however, conclusively prove that there is no change in decay time; the fluorescence enhancement does not occur due to scattering, but through higher excitation rate (excitation enhancement) due to an increase in the plasmonic near field.

Thus tuning of plasmonic modes in the UV-IR region of EM spectra through the shape-tailoring of Ag NPs can lead to coupling of specific modes with the excitation frequency of the ZnO:Er^{3+} nanoparticles and lead to fluorescence enhancement under both UV and IR excitation. A strong enhancement in fluorescence emission from ZnMgO has been reported due to the coupling interaction between the hybridized quadrupole plasmon in Ag nanoparticle aggregates, which were recognized as collections of dimers.[30] In addition, theoretical simulation demonstrated that the overlapping of the radiative quadrupolar mode with the emission band of excited fluorophores assists the fluorescence emission due to an enhancement in quantum efficiency.[32] Higher-order plasmonic multipolar modes were shown to couple with the incident EM field,[33–36] opening up possibilities to harness the higher order mode as well as the dipolar mode for fluorescence augmentation through the excitation and emission processes concurrently. Thus, in our case, the tuning of quadrupole resonance in the short wavelength region and dipole resonance in the long wavelength region is responsible for the fluorescence enhancement by Ag nanohexagons under UV and IR excitation, respectively.

The dual mode energy transfer scheme from Ag NPs to Er^{3+}–doped ZnO nanoparticles is indicated in the energy level diagram (Fig. 5). For downconversion, the energy level diagram illustrates cohesive energy transfer (ET) from Ag NPs corresponding to quadrupolar oscillations (QD) together with the direct excitations of ZnO nanoparticles under UV pump, giving rise to emission peaks in the blue-green spectral region (Fig. 5). The visible emission is a consequence of the radiative recombination of electrons–hole pairs in the intrinsic donor–acceptor pair defect states. For upconversion emission in ZnO:Er^{3+}, the absorption of a 980 nm photon by Er^{3+} ion in the ground state ($^4I_{15/2}$) elevates it to excited $^4I_{11/2}$ state, which can resonantly absorb another IR photon to go to the $^4F_{7/2}$ state. Subsequent radiative transition to the ground state or phonon-assisted relaxation to lower excited states followed by radiative transition to the ground state results in green and red UC emission, as depicted in the energy level diagram (Fig. 5). Effective ET can occur from Ag NPs corresponding to the dipolar plasmonic mode (ED) to Er^{3+}, leading to fluorescence enhancement.

Conclusions

In summary, we present a comprehensive work involving the chemical synthesis of shape-tailored silver nanoparticles for the effective tuning of surface plasmon modes and the near field generated around them, the chemical synthesis of flower-shaped Er^{3+}–doped ZnO nanoparticles, the conjugation of Ag NP–ZnO:Er^{3+} hybrid nanostructures in an appropriate configuration that leads to fluorescence enhancement in dual excitation (UV and IR) mode. Through experimental results and theoretical simulation, we have provided conclusive evidence that the fluorescence enhancement occurs due to the plasmonic effect of Ag NPs in the proximity of emitting ZnO:Er^{3+} nanoparticles. Conclusive evidence of the coupling of different plasmonic modes of Ag NPs (nano-hexagons) causing fluorescence enhancement has been established through confocal fluorescence mapping & spectroscopy of the ZnO:Er^{3+} and ZnO:Er^{3+}–Ag NP integrated system along with UV-visible absorption spectroscopy of Ag NPs; the spectra exhibit a quadrupolar peak in the UV region and a broad dipolar peak covering the near-IR region and encompassing the excitation range of ZnO:Er^{3+}. For a comprehensive understanding of the experimental results, we have used the most suitable and sophisticated simulation technique (FDTD) to estimate the near field generated by Ag NPs and their hybrids under UV and IR excitation wavelengths; these simulations demonstrated that the field enhancements are manifold compared to the incident field (Table 1) and their extinction properties. As the intensified local EM field contributes to the excitation enhancement, fluorescence enhancement

occurs. This is also proven by luminescence decay measurements showing that the decay characteristics do not change, which is a signature of excitation enhancement through the enhancement of plasmonic near field. A comprehensive correlation of the degree of fluorescence enhancement with the generated near field has been established through the FDTD simulation of an Ag nano-hexagon and its dimers at different incident wavelengths. Such dual mode fluorescence enhancement through the plasmonic mode coupling of shape-tailored Ag NPs has not been reported until now. Plasmon-mediated fluorescence enhancements in metal–semiconductor ensembles offer new possibilities in solar energy harvesting, nanobiotechnology and the lighting industry.

Acknowledgements

The authors are grateful to the CSIR TAPSUN programme for funding and to Mithun Bhomkar for help with the FDTD simulations.

Notes and references

1 M. Achermann, *J. Phys. Chem. Lett.*, 2010, **1**, 2837.
2 C. D. Geddes, *Metal enhanced fluorescence*, John Wiley & Sons, New Jersey, 2010, p. 91.
3 C. W. Lai, J. An and H. C. Ong, *Appl. Phys. Lett.*, 2005, **86**, 251105.
4 W. H. Ni, J. An, C. W. Lai, H. C. Ong and J. B. Xu, *J. Appl. Phys.*, 2006, **100**, 026103.
5 P. H. Cheng, D. S. Li, Z. Z. Yuan and D. R. Yang, *Appl. Phys. Lett.*, 2008, **92**, 041119.
6 H. Lu, X. Xu, L. Lu, M. Gong and Y. Liu, *J. Phys.: Condens. Matter*, 2008, **20**, 472202.
7 J. B. You, X. W. Zhang, Y. M. Fan, S. Qu and N. F. Chen, *Appl. Phys. Lett.*, 2007, **91**, 231907.
8 X. H. Xiao, F. Ren, X. D. Zhou, T. C. Peng, W. Wu, X. N. Peng, X. F. Yu and C. Z. Jiang, *Appl. Phys. Lett.*, 2010, **97**, 071909.
9 M. E. Aguirre, H. B. Rodríguez, E. S. Roman, A. Feldhoff and M. A. Grela, *J. Phys. Chem. C*, 2011, **115**, 24967.
10 Q. Wang, F. Song, *et al.*, *Opt. Express*, 2011, **19**(8), 6999.
11 Z. Buch, V. Kumar, H. Mamgain and S. Chawla, *Chem. Commun.*, 2013, **49**, 9845.
12 Z. Buch, V. Kumar, H. Mamgain and S. Chawla, *J. Phys. Chem. Lett.*, 2013, **4**, 3834.
13 W. Feng, *et al.*, *Chem. Commun.*, 2009, 4393.
14 F. Zhang, *et al.*, *J. Am. Chem. Soc.*, 2010, **132**, 2850.
15 S. Schietinger, *et al.*, *Nano Lett.*, 2010, **10**, 134.
16 Y. Wu, *et al.*, *J. Phys. Chem.*, 2011, **115**, 25040.
17 G. S. Meutrax and C. A. Mirkin, *Adv. Mater.*, 2005, **17**(4), 412.
18 P. Anger, P. Bharadwaj and L. Novotny, *Phys. Rev. Lett.*, 2006, **96**, 113002.
19 F. K. Guedje, M. Giloan, M. Potara, M. N. Hounkonnou and S. Astilean, *Phys. Scr.*, 2012, **86**, 055702.
20 S. A. Maier, P. G. Kik and H. A. Atwater, *Appl. Phys. Lett.*, 2002, **81**, 9.
21 W. Feng, L. D. Sun and C. H. Yan, *Chem. Commun.*, 2009, 4393–4395.
22 H. Z. Li, I. A. Ivanov, Y. Qu, Y. u. Huang and X. Duan, *Angew. Chem.*, 2010, 2865–2868.
23 A. Taflove and S. C. Hagness, *Computational Electrodynamics: The Finite-Difference Time Domain Method*, Artech House, 2000.
24 Reference Guide for FDTD Solutions, http://www.lumerical.com/fdtd, 2013.
25 E. D. Palik, *Handbook of optical constants of solids*, Academic Press, New York, 1985.
26 D. D. Evanoff Jr and G. Chumanov, *ChemPhysChem*, 2005, **6**, 1221.
27 S. A. Maier, *Plasmonics: Fundamentals and Applications*, Springer, New York, vol. 8, 2004, 80.11.
28 V. A. G. Rivera, F. A. Ferri and E. Marega Jr, *Plasmonics-Principles and Applications*, Intech, 2012, pp. 283–312.
29 H. Xu, E. J. Bjerneld, M. Kall and L. Borjesson, *Phys. Rev. Lett.*, 1999, **83**, 4357–4360.
30 H. Y. Chen, K. W. Liu, M. M. Jiang, Z. Z. Zhang, X. H. Xie, D. K. Wang, L. Liu, B. H. Li, D. X. Zhao, C. X. Shan and D. Z. Shen, *Appl. Phys. Lett.*, 2014, **104**, 091119.
31 W. Deng, L. Sudheendra, J. K. Zhao, J. Fu, D. Jin, I. M. Kennedy and E. M. Goldys, *Nanotechnology*, 2011, **22**, 325604.
32 T. Zhang, G. Lu, J. Liu, H. Shen, P. Perriat, M. Martini, O. Tillement and Q. Gong, *Appl. Phys. Lett.*, 2012, **101**, 051109.
33 F. Hao, E. M. Larsson, T. A. Ali, D. S. Sutherland and P. Nordlander, *Chem. Phys. Lett.*, 2008, **458**, 262.
34 H. Wang, Y. Wu, B. Lassiter, C. L. Nehl, J. H. Hafner, P. Nordlander and N. J. Halas, *Proc. Natl. Acad. Sci. U. S. A.*, 2006, **103**, 10856.
35 F. Hao, P. Nordlander, Y. Sonnefraud, P. V. Dorpe and S. A. Maier, *ACS Nano*, 2009, **3**, 643; Z. Yang, Z. Zhang, L. Zhang, Q. Li, Z. Hao and Q. Wang, *Opt. Lett.*, 2011, **36**, 1542.
36 S. Zhang, K. Bao, N. J. Halas, H. Xu and P. Nordlander, *Nano Lett.*, 2011, **11**, 1657.